arXiv:1408.2546v1 [physics.atom-ph] 1 Aug 2014

Propagation of two short laser pulse trains in a Λ-type three-level medium under conditions of electromagnetically induced transparency

Gabriela Buica[a,b], Takashi Nakajima[b,*]

[a] *Institute of Space Science, Bucharest-Măgurele, P.O. Box MG-23, R-77125, Romania*
[b] *Institute of Advanced Energy, Kyoto University, Gokasho, Uji, Kyoto 611-0011, Japan*

Abstract

We investigate the dynamics of a pair of short laser pulse trains propagating in a medium consisting of three-level Λ-type atoms by numerically solving the Maxwell-Schrödinger equations for atoms and fields. By performing propagation calculations with different parameters, under conditions of electromagnetically induced transparency, we compare the propagation dynamics by a single pair of probe and coupling laser pulses and by probe and coupling laser pulse trains. We discuss the influence of the coupling pulse area, number of pulses, and detunings on the probe laser propagation and realization of electromagnetically induced transparency conditions, as well on the formation of a dark state.

Keywords: laser propagation, laser pulse train, frequency comb, three-level atom, electromagnetically induced transparency
PACS: 42.50.Gy, 32.80.Qk, 42.65.Re

1. Introduction

Quantum control, sometimes referred to as coherent control, has drawn increasing interest in recent years in many different areas of physical sciences. Quantum control aims at manipulating the fate of quantum systems at will by utilizing quantum interference in one way or the other [1, 2]. The optical response of an atomic medium can be modified due to quantum interference between two different excitation pathways and an opaque optical medium can be rendered transparent to a probe field by applying an intense coupling laser field at a different frequency [3, 4]. This phenomenon has been termed electromagnetically induced transparency (EIT), and a narrow transparency window with vanished absorption and refractive index appears within an absorption line. EIT was theoretically proposed by Kocharovskaya and coworkers [5], and then it was experimentally demonstrated with Sr atoms by Harris and coworkers [6]. The basis of EIT resides in the *coherent population trapping* (CPT) in three-level Λ-type atoms, which was first discovered by Alzetta and coworkers [7] in the D lines of Na atoms: Briefly, for Λ-type atoms interacting with a probe and a coupling laser the population is trapped in the two lower states without excitation to the upper (intermediate) state during the interactions. The underlying physics of CPT is the destructive quantum interference for the transitions from the two lower states to the common upper (intermediate) states, where the establishment of coherence between the two lower states by the probe and coupling lasers is the key. Since the first experimental demonstration of EIT [6], various kinds of EIT-related phenomena have been intensively studied, some of which are lasing without inversion, nonlinear optics, sub-fs pulse generation, atomic coherence control, slow light, giant nonlinearity, and storage of light, etc. [8].

Quantum interference can be induced by lasers in many different ways. For instance the incident laser may be a single laser pulse or a *laser pulse train*. By using a comb laser, which means an ultrafast laser pulse train with a high repetition rate, one can carry out the ultrahigh resolution spectroscopy. Recently it has been shown that the *accumulation ef-*

*Corresponding author
Email addresses: buica@spacescience.ro (Gabriela Buica), t-nakajima@iae.kyoto-u.ac.jp (Takashi Nakajima)

fects of coherence by a laser pulse train play an important role for coherent control of atomic or molecular systems [9, 10]. The use of a *chirped* laser pulse train is another way for coherent control of population transfer [11]. Recent advances of laser technology allows us to actively control the amplitude and phase of the laser field from pulse to pulse, and the application of such techniques to a frequency-comb laser irradiated to a Λ-type molecule results in a robust population transfer [12].

So far most of the studies on the Λ-type system with a femtosecond laser pulse train have been done, without taking into account the propagation effects, either by assuming the presence of a stationary state [13] or a weak laser field when the lowest order perturbation theory is applicable [14]. As for the work with propagation effects taken into account, a closed Λ-type system with a degeneracy in the two lower states has been theoretically investigated with a femtosecond laser pulse train [15], when the *single* laser pulse train acts as both probe and coupling laser pulses due to the degeneracy of the system under consideration. At first glance such a degenerate Λ-type system looks very similar to a non-degenerate Λ-type system which is most commonly studied in the context of EIT. There is, however, an essential difference between them: The initial state of the former is a *mixed state* with 50:50 populations in the two degenerate lower states without coherence, while for the latter the initial state is a *pure state* and only a single state is occupied before the interactions with laser pulses. As a result, in terms of the single atom response, i.e., at the entrance to the medium, a dark state is not formed in the degenerate Λ-type system by the very first pulse, while is formed in the non-degenerate Λ-type system. As a natural consequence, we expect that the following propagation dynamics would be essentially different.

In this paper we numerically investigate the propagation dynamics of *a pair* of short laser pulse trains in a non-degenerate Λ-type atomic medium under the EIT conditions when the coupling field is stronger than the probe field. In principle such *two-colour* laser pulse trains can be produced from a single laser pulse train by the optical parametric amplification technique, etc. The pulses we assume in this paper are short, and the time interval between two successive pulses is also short compared with a lifetime of the excited state, as a result of which the spontaneous decay from the excited state will not be completed before the next pulses arrive. Unlike the case of the degenerate Λ-type system, however, this fact would play a minor role for the non-degenerate Λ-type system, since the first pulse produces a nearly perfect dark state under the conditions of EIT, at least at the entrance to the medium, and hence the population in the excited state is almost zero. The paper is organized as follows. In Section 2 we introduce the theoretical model. To describe the propagation dynamics we utilize the Maxwell-Schrödinger equations for atoms and fields and numerically solve them on a grid, assuming a one-dimensional propagation. In Section 3 we present and discuss representative numerical results for the interaction of a pair of probe and coupling laser as well as probe and coupling laser pulse trains with a three-level Λ-type atom. The question we address in this paper is whether and how much the propagation dynamics of a pair of laser pulse trains in a non-degenerate Λ-type atomic medium is different from that of a single pair of pulses under the EIT conditions. We examine the effect of the laser parameters such as coupling pulse area, number of individual pulses, and laser detunings on the temporal and spatial propagation dynamics of the probe laser pulse train. Finally, concluding remarks are given in Section 4. Atomic system of units are used throughout the present work unless otherwise stated.

2. Theoretical model

2.1. Laser pulse trains

In Fig. 1 we show the level scheme of a Λ-type atom interacting with a pair of short laser pulse trains: the state $|1\rangle$ is initially occupied, while the states $|2\rangle$ and $|3\rangle$ are initially unoccupied, and the probe (coupling) laser field resonantly couples the states $|1\rangle$ and $|2\rangle$ ($|2\rangle$ and $|3\rangle$), respectively. The transition between the states $|1\rangle$ and $|3\rangle$ is dipole-forbidden. The total electric field vector is written as

$$\mathbf{E}(z,t) = \mathbf{E}_p(z,t) + \mathbf{E}_c(z,t) \,, \tag{1}$$

where $\mathbf{E}_p(z,t)$ and $\mathbf{E}_c(z,t)$ are the probe and coupling electric field vectors that are copropagating along the z axis. Since we assume that they are in the form of pulse trains with linear polarizations which are parallel to each other, the respective fields are written as

$$\mathbf{E}_\alpha(z,t) = \mathcal{E}_{\alpha 0}\ \boldsymbol{e}\ \exp\left[i(\omega_\alpha t - k_{0\alpha} z)\right] \times \sum_{n=0}^{N_{max}-1} f_\alpha(z, t-nT) e^{in\phi} + c.c.\ , \quad (2)$$

where $\mathcal{E}_{\alpha 0}$ (with $\alpha = p$ or c hereafter) are the peak field amplitudes of the probe and coupling laser fields, respectively, and $\boldsymbol{e}$ is the polarization vector which is assumed to be identical for both lasers. $f_\alpha(z,t)$ is the slowly varying envelope, ω_α is the photon energy, and $k_{0\alpha}$ is the wavenumber in vacuum for the respective laser fields. T and N_{max} represent the time interval between two successive pulses and the number of pulses in each pulse train, respectively, which are assumed to be identical for both lasers, and ϕ is a phase shift between two successive pulses.

By taking the Fourier transform of the electric field Eq. (2) with respect to time as

$$\widetilde{E}_\alpha(z,\omega) = \int_{-\infty}^{+\infty} E_\alpha(z,t) \exp\left(-i\omega t\right) dt,$$

where the symbol $\sim$ denotes a Fourier transform, we obtain by applying the Poisson formula for $N_{max} \to \infty$, after a simple algebra,

$$\widetilde{E}_\alpha(z,\omega) = \widetilde{E}_{\alpha 0}(z, \omega - \omega_\alpha) \sum_{m=-\infty}^{+\infty} \delta(\omega - \omega_{\alpha m}), \quad (3)$$

with $\widetilde{E}_{\alpha 0}(z, \omega - \omega_\alpha) = 2\pi\ \mathcal{E}_{\alpha 0} \widetilde{f}_\alpha(\omega - \omega_\alpha)/T$ and $\omega_{\alpha m} = \omega_\alpha + \phi/T + 2\pi m/T$. The laser pulse train spectrum defined by Eq. (3) forms a frequency comb with m laser modes centered at $\omega_\alpha + \phi/T$, separated by $2\pi/T$, and with a peak amplitude $\widetilde{E}_{\alpha 0}(z, \omega - \omega_\alpha)$. Therefore the photon energy of the m^{th} mode for each pulse train is given by $(\omega_\alpha + \phi/T) \pm 2\pi m/T$. In this paper we assume that the phase shift, ϕ, is zero. As for the slowly varying envelope at the entrance to the medium, $f_\alpha(z=0,t)$, we assume that it is represented by a Gaussian function, i.e.,

$$f_\alpha(z=0,t) = e^{-\pi(t/\tau_0)^2}\ , \quad (4)$$

where τ_0 is the pulse temporal width of a single laser pulse, which is assumed to be identical for both probe and coupling lasers.

2.2. Maxwell-Schrödinger equations

As long as the pulse duration is not very short, say, if it is longer than 100 fs, we may derive the equations for atoms and fields, which are often called Maxwell-Schrödinger equations, after introducing the rotating-wave approximation and slowly varying envelope approximation (SVEA). In SVEA the envelope of the electric field varies slowly in time and space compared to the optical period and the wavelength of the field, and therefore the second order derivative terms are negligible, i.e., $|\partial_z^2 f_\alpha(z,t)| \ll k_{0\alpha} |\partial_z f_\alpha(z,t)|$ and $|\partial_t^2 f_\alpha(z,t)| \ll \omega_\alpha |\partial_t f_\alpha(z,t)|$, where ∂_z and ∂_t represent the derivatives relative to the variables z and t.

As for the response of the single atom to the laser fields, we can follow the standard procedure and easily derive the time-dependent Schrödinger equations in terms of the probability amplitudes of the relevant states described in Fig. 1. Since we couple those equations with the Maxwell equations in what follows, it is more convenient to introduce a moving frame by replacing the space and time variables in the laboratory frame, z and t, by those in the moving frame, ζ and τ, through the relations of $\zeta = z$ and $\tau = t - z/c$, where c is the speed of light. Finally, we obtain the following probability amplitude equations

$$\frac{\partial}{\partial\tau} c_1(\zeta,\tau) = \frac{i}{2}\Omega_p(\zeta,\tau) c_2(\zeta,\tau), \quad (5)$$

$$\frac{\partial}{\partial\tau} c_2(\zeta,\tau) = -(i\delta_p + \gamma) c_2(\zeta,\tau) + \frac{i}{2}\Omega_p(\zeta,\tau) c_1(\zeta,\tau) + \frac{i}{2}\Omega_c(\zeta,\tau) c_3(\zeta,\tau), \quad (6)$$

$$\frac{\partial}{\partial\tau} c_3(\zeta,\tau) = -i(\delta_p - \delta_c) c_3(\zeta,\tau) + \frac{i}{2}\Omega_c(\zeta,\tau) c_2(\zeta,\tau), \quad (7)$$

where $c_k(\zeta,\tau)$ ($k = 1, 2,$ and 3) is the slowly varying probability amplitude of state $|k\rangle$ with the initial conditions of $c_1(\zeta, \tau = -\infty) = 1$ and $c_k(\zeta, \tau = -\infty) = 0$ ($k = 2,\ 3$), γ is the spontaneous decay rate of state $|2\rangle$, and δ_p and δ_c are the detunings of the probe and coupling lasers, respectively. $\Omega_p(\zeta,\tau)$ and $\Omega_c(\zeta,\tau)$ are the one-photon Rabi frequency due to the probe and coupling laser pulse trains, and are defined as

$$\Omega_p(\zeta,\tau) = \Omega_{p0} \sum_{n=0}^{N_{max}-1} f_p(\zeta, \tau - nT), \quad (8)$$

$$\Omega_c(\zeta,\tau) = \Omega_{c0} \sum_{n=0}^{N_{max}-1} f_c(\zeta, \tau - nT), \quad (9)$$

with the peak value of $\Omega_{p0} = d_{12}\mathcal{E}_{p0}$ ($\Omega_{c0} = d_{23}\mathcal{E}_{c0}$), where d_{12} (d_{23}) is the one-photon dipole moment for the transition between states $|1\rangle$ and $|2\rangle$ ($|2\rangle$ and $|3\rangle$), respectively.

As for the response of the laser fields to the atomic medium we obtain the following Maxwell equations

$$\frac{\partial}{\partial\zeta}\Omega_p(\zeta,\tau) = -2i\mu_p c_2^*(\zeta,\tau)c_1(\zeta,\tau), \quad (10)$$

$$\frac{\partial}{\partial\zeta}\Omega_c(\zeta,\tau) = -2i\mu_c c_2^*(\zeta,\tau)c_3(\zeta,\tau), \quad (11)$$

where μ_p (μ_c) is the medium propagation coefficient for the probe (coupling) laser, which is defined as $\mu_p = N_d\omega_p|d_{12}|^2/2\varepsilon_0 c$ ($\mu_c = N_d\omega_c|d_{23}|^2/2\varepsilon_0 c$), where N_d is the atomic density of the medium and ε_0 is the vacuum permittivity. The initial conditions for Eqs. (10)-(11) are given by Eqs. (4), (8) and (9).

Now, we solve the coupled differential Eqs. (5)-(7), (10) and (11) for the atoms and laser fields with arbitrary temporal shapes and field strengths. This is a complicated mathematical problem and there is no analytical solution for the general case. Therefore we resort to the numerical method based on the Crank-Nicholson algorithm which has a second order accuracy in both time and space. The computer code we have developed for this problem is an extension of our previous work for the propagation of phase-controlled two-colour lasers in a two-level medium [16].

2.3. Maxwell-Schrödinger equations in the dressed state basis

A more convenient way to study the Maxwell-Schrödinger equations is to use the dressed state basis [17], by taking the advantage of the *dark* and *bright* states, $|D\rangle$ and $|B\rangle$, defined as coherent asymmetric and symmetric superposition of the two lower bare states, $|1\rangle$ and $|3\rangle$, $|D\rangle = (\Omega_{c0}|1\rangle - \Omega_{p0}|3\rangle)/\Omega_{B0}$ and $|B\rangle = (\Omega_{p0}|1\rangle + \Omega_{c0}|3\rangle)/\Omega_{B0}$, where $\Omega_{B0} = \sqrt{\Omega_{p0}^2 + \Omega_{c0}^2}$ represents the bright Rabi frequency. The *dark* and *bright* probability amplitudes, c_D and c_B, are now calculated in terms of c_1 and c_3,

$$c_D(\zeta,\tau) = \frac{1}{\Omega_{B0}}[\Omega_{c0}c_1(\zeta,\tau) - \Omega_{p0}c_3(\zeta,\tau)], \quad (12)$$

$$c_B(\zeta,\tau) = \frac{1}{\Omega_{B0}}[\Omega_{p0}c_1(\zeta,\tau) + \Omega_{c0}c_3(\zeta,\tau)]. \quad (13)$$

Similarly, we define new field variables [17], $\Omega_D(\zeta,\tau)$ and $\Omega_B(\zeta,\tau)$, the *dark* and *bright* fields, calculated in terms of Ω_p and Ω_c, as

$$\Omega_D(\zeta,\tau) = \frac{1}{\Omega_{B0}}[\Omega_{c0}\Omega_p(\zeta,\tau) - \Omega_{p0}\Omega_c(\zeta,\tau)], \quad (14)$$

$$\Omega_B(\zeta,\tau) = \frac{1}{\Omega_{B0}}[\Omega_{p0}\Omega_p(\zeta,\tau) + \Omega_{c0}\Omega_c(\zeta,\tau)]. \quad (15)$$

First, by taking the derivative of Eqs. (12) and (13) with respect to time, τ, and using the probability amplitude equations (5)-(7) and dressed fields' definitions (14) and (15) we obtain the following set of probability amplitude equations in the new basis of the dressed states:

$$\frac{\partial}{\partial\tau}c_D(\zeta,\tau) = \frac{i}{2}\Omega_D(\zeta,\tau)c_2(\zeta,\tau) - i(\delta_p - \delta_c)\frac{\Omega_{p0}}{\Omega_{B0}^2}\left[\Omega_{c0}c_B(\zeta,\tau) + \Omega_{p0}c_D(\zeta,\tau)\right], \quad (16)$$

$$\frac{\partial}{\partial\tau}c_2(\zeta,\tau) = -(i\delta_p + \gamma)c_2(\zeta,\tau) + \frac{i}{2}\Omega_B(\zeta,\tau)c_B(\zeta,\tau) + \frac{i}{2}\Omega_D(\zeta,\tau)c_D(\zeta,\tau), \quad (17)$$

$$\frac{\partial}{\partial\tau}c_B(\zeta,\tau) = \frac{i}{2}\Omega_B(\zeta,\tau)c_2(\zeta,\tau) - i(\delta_p - \delta_c)\frac{\Omega_{c0}}{\Omega_{B0}^2}\left[\Omega_{p0}c_B(\zeta,\tau) + \Omega_{c0}c_D(\zeta,\tau)\right], \quad (18)$$

with the initial conditions $c_D(\zeta,\tau = -\infty) = \Omega_{c0}/\Omega_{B0}$, $c_2(\zeta,\tau = -\infty) = 0$, and $c_B(\zeta,\tau = -\infty) = \Omega_{p0}/\Omega_{B0}$, as the Λ-type atom is initially prepared in the ground state. Second, by taking the derivative of Eqs. (14) and (15) with respect to ζ and using Eqs. (10)-(13) we get after a simple algebra the following Maxwell equations in the dressed state basis:

$$\frac{\partial}{\partial\zeta}\Omega_D(\zeta,\tau) = -2ic_2^*(\zeta,\tau) \times \left[\mu_{B1}c_D(\zeta,\tau) + \mu_D c_B(\zeta,\tau)\right], \quad (19)$$

$$\frac{\partial}{\partial\zeta}\Omega_B(\zeta,\tau) = -2ic_2^*(\zeta,\tau) \times \left[\mu_D c_D(\zeta,\tau) + \mu_{B2}c_B(\zeta,\tau)\right], \quad (20)$$

where the new propagation coefficients μ_{B1}, μ_{B2} and μ_D are defined as $\mu_{B1} = (\Omega_{c0}^2\mu_p + \Omega_{p0}^2\mu_c)/\Omega_{B0}^2$, $\mu_{B2} = (\Omega_{p0}^2\mu_p + \Omega_{c0}^2\mu_c)/\Omega_{B0}^2$, and $\mu_D = (\mu_p - \mu_c)\Omega_{p0}\Omega_{c0}/\Omega_{B0}^2$, respectively. For initially matched probe and coupling pulses at the entrance to the medium, $f_p(\zeta = 0,\tau) = f_c(\zeta = 0,\tau)$, the initial conditions satisfied by the dressed fields are evaluated from Eqs. (14) and (15) as $\Omega_D(\zeta = 0,\tau) = 0$ and $\Omega_B(\zeta = 0,\tau) = \Omega_{B0}\sum_n f_p(\zeta = 0, \tau - nT)$.

Finally, because we are interested in a weak interaction of the probe field with the atom, $\Omega_{p0} \ll \Omega_{c0}$, important simplifications of the probability amplitude Eqs. (16)-(18) occur as follows,

$$\frac{\partial}{\partial\tau}c_D(\zeta,\tau) \simeq 0, \quad (21)$$

$$\frac{\partial}{\partial\tau}c_2(\zeta,\tau) \simeq -(i\delta_p + \gamma)c_2(\zeta,\tau) + \frac{i}{2}\Omega_B(\zeta,\tau)c_B(\zeta,\tau), \quad (22)$$

$$\frac{\partial}{\partial\tau}c_B(\zeta,\tau) \simeq -i(\delta_p - \delta_c)c_D(\zeta,\tau) + \frac{i}{2}\Omega_B(\zeta,\tau)c_2(\zeta,\tau), \quad (23)$$

with the initial conditions $c_D(\zeta,\tau = -\infty) \simeq 1$, $c_2(\zeta,\tau = -\infty) = 0$, and $c_B(\zeta,\tau = -\infty) \simeq 0$, showing that the Λ-type atom is initially in a dark state $|D\rangle$. Obviously, Eqs. (21)-(23) correspond to a Λ-type atom where the dressed state $|D\rangle$ is practically decoupled from the two fields and the dark field is, accordingly to its definition (14), $\Omega_D(\zeta,\tau) \simeq 0$, reducing thus the problem of a three- to a two-level atom. Hence, for initially matched pulses in the limit of weak probe field, $\Omega_{p0} \ll \Omega_{c0}$, we obtain that the atomic system reaches a dark state where $\Omega_D(\zeta,\tau) \simeq 0$ and the temporal profile of probe and coupling laser pulses does not change at any optical depth, $f_p(\zeta,\tau) = f_c(\zeta,\tau) = f_p(\zeta = 0,\tau)$, and therefore the medium becomes transparent to both lasers [17].

Similar simplifications exist for the Maxwell Eqs. (19) and (20) in the limit of weak probe field, where the propagation coefficients simplify as $\mu_{B1} \simeq \mu_p$, $\mu_{B2} \simeq \mu_c$, and $\mu_D \simeq 0$. Substituting the above simplified propagation coefficients in the Maxwell Eqs. (19) and (20) we obtain

$$\frac{\partial}{\partial\zeta}\Omega_D(\zeta,\tau) \simeq -2i\mu_p c_2^*(\zeta,\tau)c_D(\zeta,\tau), \quad (24)$$

$$\frac{\partial}{\partial\zeta}\Omega_B(\zeta,\tau) \simeq -2i\mu_c c_2^*(\zeta,\tau)c_B(\zeta,\tau). \quad (25)$$

Next, because the atom interacts with two laser pulse trains, whose spectra consist of combs with different frequencies, is useful to consider the above Maxwell-Schrödinger equations (21)-(25) in the spectral domain where the dependence on the frequency comb modes is emphasized. By taking the Fourier transform of Eqs. (21)-(23) with respect to τ and using the Fourier transform of the probability amplitude $c_k(\zeta,t)$ ($k = B, D$ and 2) defined as

$$\widetilde{c}_k(\zeta,\omega) = \int_{-\infty}^{+\infty} c_k(\zeta,\tau')e^{-i\omega\tau'}d\tau', \quad (26)$$

we can write, after a straightforward algebra, the set of probability amplitude equations in the spectral domain as follows,

$$\widetilde{c}_D(\zeta,\omega) \simeq 0, \quad (27)$$

$$\widetilde{c}_2(\zeta,\omega) \simeq \frac{1}{2(\omega + \delta_p - i\gamma)} \times \sum_{m=-\infty}^{+\infty} \widetilde{\Omega}_{B0}(\zeta, m\omega_r)\widetilde{c}_B(\zeta,\omega - m\omega_r), \quad (28)$$

$$\widetilde{c}_B(\zeta,\omega) \simeq \frac{1}{2(\omega + \delta_p - \delta_c)} \times \sum_{m=-\infty}^{+\infty} \widetilde{\Omega}_{B0}(\zeta, m\omega_r)\widetilde{c}_2(\zeta,\omega - m\omega_r), \quad (29)$$

where we employ the Fourier transform of the bright Rabi field, $\widetilde{\Omega}_B(\zeta,\omega)$, given by

$$\widetilde{\Omega}_B(\zeta,\omega) = \int_{-\infty}^{+\infty} \Omega_B(\zeta,\tau')e^{-i\omega\tau'}d\tau' = 2\pi\,\widetilde{\Omega}_{B0}(\zeta,\omega)\sum_{m=-\infty}^{+\infty}\delta(\omega - m\omega_r),$$

with

$$\widetilde{\Omega}_{B0}(\zeta,\omega) = [\Omega_{p0}\widetilde{\Omega}_{p0}(\zeta,\omega) + \Omega_{c0}\widetilde{\Omega}_{c0}(\zeta,\omega)]/\Omega_{B0},$$

$$\widetilde{\Omega}_{p0}(\zeta,\omega) = d_{12}\mathcal{E}_{p0}\widetilde{f}_p(\zeta,\omega)/T,$$

$$\widetilde{\Omega}_{c0}(\zeta,\omega) = d_{23}\mathcal{E}_{c0}\widetilde{f}_c(\zeta,\omega)/T,$$

where $\omega_r = 2\pi/T$ represents the repetition angular frequency. For the EIT parameters we employ, is quite visible from the amplitude probabilities Eqs. (27)-(29), that the upper and bright state populations, $|\widetilde{c}_k(\zeta,\omega)|^2$ $(k = 2, B)$, are periodic functions with the same periodicity as the laser frequency comb ω_r.

By taking now the Fourier transform of Eqs. (24) and (25) and using Eq. (27) the Maxwell equations in the spectral domain reads as

$$\frac{\partial}{\partial\zeta}\widetilde{\Omega}_D(\zeta,\omega) \simeq 0, \tag{30}$$

$$\frac{\partial}{\partial\zeta}\widetilde{\Omega}_B(\zeta,\omega) \simeq -i\frac{\mu_c}{\pi}\,\widetilde{c}_2^*(\zeta,\omega)\otimes\widetilde{c}_B(\zeta,\omega), \tag{31}$$

where the symbol $\otimes$ denotes the convolution operator which is defined as $h(\omega)\otimes g(\omega) = \int_{-\infty}^{+\infty} h(\omega-\omega')g(\omega')d\omega'$. In the limit of weak probe field for initially matched pulses, similar to the findings in the temporal domain, is clear from Eq. (30) that the atomic system reaches a dark state where $\widetilde{\Omega}_D(\zeta,\omega) \simeq 0$ and the probe and coupling laser pulses achieve identical spectral profiles $\widetilde{f}_p(\zeta,\omega) = \widetilde{f}_c(\zeta,\omega)$.

3. Numerical Results and Discussions

In this section we present representative results for the propagation of the short probe and coupling laser pulse trains in a Λ-type atomic medium by numerically solving Eqs. (5)-(11). We consider realistic values for the atomic and lasers parameters and represent the propagation length in units of $\mu_p\zeta$ which is the so-called optical depth [18]. The population of state $|k\rangle$ $(k = 1, 2,$ and $3)$ at any time and space, (ζ,τ), is calculated as $P_k(\zeta,\tau) = |c_k(\zeta,\tau)|^2$. Atomic coherence between states $|1\rangle$ and $|2\rangle$ is defined by $c_1(\zeta,\tau)c_2^*(\zeta,\tau)$, where the real part, $\mathrm{Re}[c_1(\zeta,\tau)c_2^*(\zeta,\tau)]$, stands for the refractive index and the imaginary part, -$\mathrm{Im}[c_1(\zeta,\tau)c_2^*(\zeta,\tau)]$, stands for the absorption coefficient, respectively. The dark and bright state populations are calculated as $P_D(\zeta,\tau) = |c_D(\zeta,\tau)|^2$ and $P_B(\zeta,\tau) = |c_B(\zeta,\tau)|^2$. In what follows we present the propagation of a single pair of resonant probe and coupling laser pulses, next we discuss the propagation of resonant probe and coupling laser pulse trains, and finally we investigate the influence of symmetric and asymmetric detunings on the propagation of laser pulse trains.

3.1. Propagation of a single pair of resonant probe and coupling laser pulses

To start with, we investigate the propagation of a *single* pair of probe and coupling laser pulses, i.e., $N_{max} = 1$ in Eq. (2), with different pulse durations and laser intensities. Representative results for the temporal shape of the probe pulse $\Omega_p(\zeta,\tau)$ at different optical depths $\mu_p\zeta = 0$, 3, 6, and 9 ps^{-1} are shown in Figs. 2(a)-(e) where the pulse durations of both probe and coupling laser pulses are 100 fs, 1 ps, 10 ps, 100 ps, and 1 ns, respectively. The parameters we have chosen for Fig. 2 are $\Omega_{p0} = 0.04$ THz and $\Omega_{c0} = 1$ THz for the Rabi frequencies, $\tau_0 = 1$ ps for the pulse duration, $\delta_p = \delta_c = 0$ for detunings, and the spontaneous decay rate from the upper state is $\gamma = 70$ MHz. Similar results, but at higher coupling laser intensities, are shown in Figs. 2(f)-(j) with $\Omega_{c0} = 10$ THz. We note in Fig. 2 the quite different spatio-temporal changes of the probe pulse with short pulse durations compared to those with long pulse durations for which most of the EIT studies have been carried out. As we see in Figs. 2(a)-(c) and Figs. 2(f)-(g) for small and moderate coupling pulse areas $(\Omega_{c0}\tau_0 < 10)$ the probe laser pulse is significantly distorted during the propagation, and each pulse breaks up into several sub-pulses with positive and negative amplitudes [16, 19, 20]. The number of modulations at the trailing edge of the pulse increases as the propagation distance (or optical depth) increases. We note that, if the pulse area is small and the pulse duration is shorter than the lifetime of the upper state, the propagation of the laser pulse does not obey the exponential absorption given by the Beer's law (we should recall that the Beer's law is valid for constant laser fields) [21]. Therefore the right wing (or trailing edge) of laser pulses can propagate for longer distances [19]. When the pulse durations are as short as sub-ps or ps and the pulse areas, in particular the pulse areas of the coupling laser pulses, are also small, there is no EIT effect. In such cases we simply observe the modulations at the trailing edge of the probe pulse [16, 19], as shown in Figs. 2(a) and (b). As the pulse durations become longer and accordingly the pulse areas become larger, EIT

is established with the so-called preparation loss at the leading edge of the pulse [17], as shown in Figs. 2(d) and (e). If we increase the peak intensities of the coupling laser pulse by ten times, $\Omega_{c0} = 10$ THz, (right column of Fig. 2) we observe similar dynamics but at shorter pulse durations.

For a better understanding of the break-up process of the small area pulse, we plot in Figs. 3(a)-(c) and Figs. 3(d)-(f) the temporal shape of the probe pulse, $\Omega_p(\zeta, \tau)$, and the population in the ground state, $P_1(\zeta, \tau)$, respectively, at two different optical depths $\mu_p\zeta = 0$ and 1 ps^{-1} for the case of a single laser pulse propagating in a *two-level medium*, i.e., $N_{max} = 1$ and $\Omega_{c0} = 0$. The parameters we choose for Fig. 3 are $\Omega_{p0} = 0.04$ THz, $\tau_0 = 5$ ps, and $\delta_p = 0$ with three different spontaneous decay rates of $\gamma = 700$ GHz ($\gamma^{-1} = 1.4$ ps), 70 GHz ($\gamma^{-1} = 14$ ps), and 7 GHz ($\gamma^{-1} = 140$ ps) for Figs. 3(a) and (d), Figs. 3(b) and (e), and Figs. 3(c) and (f), respectively. It is well known that in the weak field regime, when the Rabi frequency is smaller than the atomic linewidth, $\Omega_{p0} < \gamma$ shown in Fig. 3(a), the laser pulse is damped and strongly absorbed, while in the strong field regime, $\Omega_{p0} > \gamma$ in Fig. 3(c), the laser pulse oscillates and reshapes due to the Rabi flopping between the ground and excited state populations. Since we are using laser pulses we should also take into consideration the pulse duration [19]. As we see in Fig. 3(a), the pulse is absorbed by the medium if the lifetime of state $|2\rangle$ is short compared with the pulse duration ($\gamma\tau_0 = 3.5$). If the lifetime of state $|2\rangle$ is longer than the pulse duration ($\gamma\tau_0 = 0.035$), the trailing edge of the pulse modulates with positive and negative amplitudes, as shown in Figs. 3(b) and (c). The modulations of the trailing edge of the pulse are spread over for a time scale of the order of γ^{-1} [17].

3.2. Propagation of probe and coupling laser pulse trains with zero detunings

Next, we study the propagation of the probe and coupling *laser pulse trains*, i.e., $N_{max} > 1$ in Eq. (2). In Fig. 4 we plot the spatio-temporal change of the probe laser field $\Omega_p(\zeta, \tau)$, at different optical depths $\mu_p\zeta = 0$, 3, 6, and 9 ps^{-1}, for the first, 40^{th}, and 120^{th} pulses in the probe pulse train. The probe and coupling laser pulse trains are initially matched with identical pulse envelopes at the entrance to the medium. The parameters we employ for Fig. 4 are $\Omega_{p0} = 0.04$ THz, $\Omega_{c0} = 0.5$ THz, $\delta_p = \delta_c = 0$, $\tau_0 = 1$ ps and $T = 10$ ns. The frequency separation between two successive comb teeth is 0.2π GHz and the spontaneous decay rate from the upper state is $\gamma = 70$ MHz, i.e., 14 ns lifetime. As mentioned before the pulse duration of each individual pulse, τ_0, is much shorter than the lifetime of the upper state and there is no enough time for a complete decay of the upper excited state $|2\rangle$ before the next pulse in the train arrives. Under these conditions, the area of each of the individual probe laser pulse is small while that of the coupling laser pulse is moderate, i.e., $\Omega_{p0}\tau_0 = 0.04$ and $\Omega_{c0}\tau_0 = 0.5$. What we learn from Fig. 4 is that, although EIT is not yet established when the first probe pulse goes through the medium, coherence is slowly accumulated in the medium as more probe and coupling pulses interact with the medium, and when the 120^{th} probe pulse enters the medium we can see the some signature of EIT. We note that our numerical results for atomic populations and probe laser absorption at the entrance to the medium (not shown here) agree well with the results presented in [22] in terms of a single atom response under the presence of a probe laser train pulse and a continuous-wave coupling laser.

What we glimpse in Fig. 4 is indeed an EIT effect by the pair of probe and coupling laser pulse trains but with different degrees of transparencies. This interpretation can be verified by looking at the populations of the *dark* and *bright* states. In Fig. 5 we show the variations of the dark and bright state populations $P_D(\zeta, \tau)$ and $P_B(\zeta, \tau)$ as a function of time at different optical depths. As expected, the dark state population induced by the very first pulse is nearly unity at the entrance to the medium. This is quite in contrast to the case of a degenerate Λ-type system in which coherence between the two lower states induced by the very first pulse is negligibly small, for example, as shown in the red side panel of the upper left figure of Fig. 6 in [15]. Since we find out that the single atom response (at optical depth = 0) by the first pulse is clearly different for the non-degenerate and degenerate Λ-type systems, we expect that the following propagation dynamics should be quite different as well. Now, back to Fig. 5 in this paper, we notice that the dark state population becomes slightly smaller as the optical depth becomes larger for a fixed number of irradiated pulses, say, 50, indicating that the transparency slightly deteriorates for larger optical depths, at least up to $\mu_p\zeta = 9$ ps^{-1}. Clearly this deterioration of transparency is due to the propagation effects. In addition we compare in Figs. 6(a) and (b) the population dynamics of states $|1\rangle$ and

$|3\rangle$, $P_1(\zeta,\tau)$ and $P_3(\zeta,\tau)$, at different optical depths $\mu_p\zeta = 0$, 3, 6 and 9 ps^{-1}. All the parameters are chosen to be the same with those for Fig. 4. It is clear that a steady dark state is reached only at the entrance to the medium ($\mu_p\zeta = 0$) after irradiation with more than 60 pulses when both populations P_1 and P_3 (solid lines in Fig. 6) are time independent.

Next, we increase the coupling laser intensity so that $\Omega_{c0} = 1$ THz and hence the pulse area of the individual coupling laser pulse is $\Omega_{c0}\tau_0 = 1$, while keeping all other parameters exactly the same with those for Fig. 4. The results are shown in Fig. 7 for the first, 40^{th}, and 120^{th} pulses in the probe pulse train. Clearly, compared with the case of Fig. 4, the transmission of the probe laser pulses becomes much better and for the 120^{th} pulse we see an ideal EIT effect where the probe laser pulse train propagates without absorption. The probe laser absorption for the 120^{th} pulse (not shown here) takes negligible values for optical depths at least up to 9 ps^{-1}. Similar to Fig. 5 for $\Omega_{c0} = 0.5$ THz, we present in Fig. 8 the dark and bright state populations $P_D(\zeta,\tau)$ and $P_B(\zeta,\tau)$ for $\Omega_{c0} = 1$ THz as a function of time at different optical depths. We notice that the steady dark state population for $\Omega_{c0} = 1$ THz is much closer to unity compared with the case of $\Omega_{c0} = 0.5$ THz, which indicates that even if the probe and coupling laser pulses are short and form pulse trains, more ideal EIT is realized by increasing the coupling laser intensity. Clearly, after the irradiation of tens of pulses the Λ-type atomic medium already reaches the steady dark state, and the temporal profile of the probe pulse is hardly changed and the absorption of the probe pulses is almost negligible at any optical depths.

Finally, in Figs. 9(a) and (b) we compare the population dynamics of states $|1\rangle$ and $|3\rangle$, $P_1(\zeta,\tau)$ and $P_3(\zeta,\tau)$, at different optical depths $\mu_p\zeta = 0$, 3, 6 and 9 ps^{-1}. All the parameters are chosen to be the same with those for Fig. 7. A notable difference is seen between the results for $\Omega_{c0} = 1$ THz [Figs. 9(a) and (b)] and 0.5 THz [Figs. 6(a) and (b)]: for $\Omega_{c0} = 1$ THz the populations P_1 and P_3 are time independent at different optical depths after the irradiation with many pulses (approximately 120), and they take almost the same values at any optical depth. Therefore the population is trapped in a steady dark state, which is a superposition of the two lower states $|1\rangle$ and $|3\rangle$, and the upper state $|2\rangle$ remains practically unpopulated that give rise to propagation without absorption in Fig. 7. For moderate coupling pulse area $\Omega_{c0}\tau_0 = 1$ the time scale to establish the ideal EIT and the generation of a dark state is of the order of a few microseconds, while for larger coupling pulse areas the EIT is established much faster in the nanoseconds regime.

3.3. Propagation of probe and coupling laser pulse trains with symmetric and asymmetric detunings

Before closing this section we investigate how the laser detunings influence the propagation dynamics of the probe laser pulse train. Note that for all results presented until now in this paper, the central comb teeth of both probe and coupling lasers are on exact resonance, i.e., $\delta_p = \delta_c = 0$. As mentioned before, the spectrum of a laser pulse train forms a frequency comb with teeth which are separated by $2\pi/T$ and, in particular, for a pulse train with a single pulse duration of 1 ps and time interval of 10 ns the separation between the two successive comb teeth is 0.2π GHz.

We consider two different choices of detunings for the probe and coupling lasers as illustrated in Figs. 10(a) and (b), which we call *symmetric* and *asymmetric detunings*, respectively. For the symmetric detunings, all comb teeth of the probe and coupling laser pulses match, i.e., $\delta_p = \delta_c$, and the question is which comb teeth are on exact resonance with the $|1\rangle$-$|2\rangle$ and $|2\rangle$-$|3\rangle$ transitions. For the asymmetric detunings, the comb teeth of the probe and coupling lasers at the opposite side with respect to the central peak in the frequency domain match, i.e., $\delta_p = -\delta_c$. Note that only one pair of the probe and coupling comb teeth is on exact resonance with the corresponding transitions, as depicted in Figs. 10(a) and (b), provided that the values of the probe and coupling detunings are $\delta_p = m_p\ \omega_r$ ($\delta_c = m_c\ \omega_r$), with m_p (m_c) an integer. Therefore whatever the difference we might see between them in terms of probe pulse propagation arises from the contributions of other comb teeth which are off resonance.

In Fig. 11 we compare the spatio-temporal changes of the absolute value of probe laser field $|\Omega_p(\zeta,\tau)|$ for the above choices of detunings of the probe and coupling lasers: (a) *symmetric detunings* $\delta_p = \delta_c \simeq 201.062$ GHz (blue lines) and (b) *asymmetric detunings* $\delta_p = -\delta_c \simeq 201.062$ GHz (red lines), for the first (upper graph of Fig. 11), 10^{th} (middle graph of Fig. 11), and 20^{th} (lower graph of Fig. 11) pulses. The symmetric (asymmetric) detunings correspond to the $m_p = m_c = 320$ ($m_p = -m_c = 320$) comb teeth of the probe and

coupling lasers and we increase the coupling laser intensity such that $\Omega_{c0} = 2$ THz. All the rest of the parameters employed in Fig. 11 are the same with those for Fig. 4. Clearly, we see some differences between the two cases, especially in the trailing edge of the probe pulse, where the optical ringing [23, 24] occur for both cases, however the oscillations in the trailing edge disappear for symmetric detunings case for larger t/T because a steady dark state is reached quite fast after the interaction with the first 20 pulses for optical depths $\mu_p\zeta < 6$ ps^{-1}. As mentioned before, these differences come from the contribution of all other off-resonant comb modes of both lasers, Fig. 10(b) for the asymmetric case.

Accordingly, the dynamics of the dark and bright state populations $P_D(\zeta,\tau)$ and $P_B(\zeta,\tau)$ is quite different in both cases, as shown in Fig. 12. For the symmetric detunings case the medium reaches a steady dark state from the very beginning in terms of the number of pulses and optical depths (blue lines in Fig. 12) and the dark and bright state populations slightly oscillate toward the establishment of EIT, while for the asymmetric detunings the populations of both dark and bright states exhibit a sew-saw pattern (red lines in Fig. 12) with envelopes that follow the profile of the dark and bright state populations for symmetric detunings. The oscillatory behavior of the dark and bright state populations for asymmetric detunings is the result of the Rabi oscillations of the probability amplitude of state $|3\rangle$, $c_3(\zeta,\tau)$, that enters in the definitions of the dark and bright states Eqs. (12) and (13). The number of Rabi oscillations of $c_3(\zeta,\tau)$ during a single pulse duration is proportional with the two-photon Raman detuning, $\delta_p - \delta_c$, and depends on the comb modes order. One of the conditions required to establish a dark state in case of a single pair of probe and coupling pulses is the two-photon Raman resonance, but the EIT effect occurs over a small transparency frequency window, while for a train of laser pulses the best EIT effect occur, whenever all the probe and coupling comb teeth match ($\delta_p = \delta_c = m_p\ \omega_r$), within a larger transparency window as shows the population of the excited state P_2, in Fig. 13, as a function of the probe laser detuning at entrance to the medium (blue dashed lines for symmetric detunings). The laser parameters in Fig. 13 are the same as in Fig. 11 and the detuning dependence of the population of the upper excited state at $\mu_p\zeta = 0$ for a single pair of probe and coupling pulses ($N_{max} = 1$) is compared to that of the probe and coupling laser pulse trains ($N_{max} = 2, 4, 10$, and 20). For the asymmetric detunings case, although the two-photon Raman detuning is not zero but multiple of the repetition angular frequency, $\delta_p - \delta_c = 2\ m_p\ \omega_r$, the atomic system also exhibits some degree of transparency within a smaller transparency window (red lines in Fig. 13 for asymmetric detunings). However it is clear from Fig. 13 that EIT is better established for the case of symmetric detunings.

Of course there are many other choices for the probe and coupling laser detunings, and the above choices are the two special cases we present. Obviously, larger differences between pulse propagations with symmetric and asymmetric detunings are obtained for energies that do not satisfy the one-photon resonance condition [9], since the two-photon Raman resonance is always fulfilled for symmetric detunings. There is one exception, when a similar behavior of the pulse propagation leading to EIT is obtained for asymmetric detunings that do not correspond to one-photon resonance, $\delta_p = -\delta_c = (2\ m_p + 1)\ \omega_r/2$, because the two-photon Raman detuning is again a multiple of the repetition angular frequency and therefore the two-photon resonance condition is satisfied, as shows, in Fig. 13, the population of the excited state for detunings that are odd multiples of $\omega_r/2$. In contrast with our findings for the Λ-type atom we expect that the asymmetric detunings case should give the best EIT for a three level ladder-type atom when the two-photon detuning dependence of the probability amplitude of state $|3\rangle$ in Eq. (7) is given by $\delta_p + \delta_c$.

4. Conclusions

We have systematically studied the propagation of a pair of short laser pulse trains in a three-level Λ-type atomic medium by simultaneously solving the Maxwell-Schrödinger equations. First, for a single pair of probe and coupling pulses we have presented in Fig. 2 the different spatio-temporal changes of the probe pulse with short duration (fs and ps) compared to those with long duration (ns) for different coupling laser strengths. For long pulse durations (ns) the oscillations of the probe pulse during the propagation take place at the leading edge of the pulse and are induced by the Rabi oscillations between the $|1\rangle$ and $|3\rangle$ levels. The EIT effect for long pulse durations is established at large pulse areas provided that $\Omega_{c0} >> \Omega_{p0}$. In contrast, for short

pulse durations (fs or ps) and small pulse areas the trailing edge of the probe laser pulse is significantly distorted during the propagation and the right wing of the pulse breaks up into several sub-pulses. As the coupling pulse area increases the amplitude of the sub-pulses is reduced, the probe laser propagates undistorted and an ideal EIT is established. A second goal of this work is to compare, *for short pulses (ps)*, the propagation dynamics of a pair of probe and coupling laser pulse trains with a single pair of probe and coupling laser pulses under the conditions of EIT. The main difference is that for a single pair of probe and coupling lasers the EIT is accomplished for *large coupling pulse areas* ($\Omega_{c0}\tau_0 > 10^3$), while for propagation of probe and coupling laser pulse trains the EIT (as well the formation of a dark state), is reached for *moderate coupling pulse areas* ($\Omega_{c0}\tau_0 > 1$), and it strongly depends on the number of pulses in the train, as shown in Fig. 7. We have discussed how the propagation dynamics of the laser pulse trains through the medium under the EIT conditions could be modified by the appropriate choice of laser parameters such as Rabi frequencies, pulse durations, number of pulses, and laser detunings. Because of the use of short ps laser pulse trains and moderate coupling field intensities, realization of EIT has been found to be more demanding with ps train pulses compared with the case of irradiation with a single pair of ns pulses. However, after the medium interacts with a few tens of pulses at moderate coupling field intensities EIT can be achieved. We have shown that the attainment of EIT can be manipulated, depending on which pairs of comb teeth are on resonance and a steady dark state can be achieved whenever the two-photon detuning is an integer of the repetition angular frequency ω_r.

5. Acknowledgment

This work was supported by a Grant-in-Aid for scientific research from the Ministry of Education and Science of Japan. The work by G.B. was partially supported by a research program Laplas 3 from the National Authority for Scientific Research. G.B. acknowledges the hospitality and the financial aid during her stay at Kyoto University where a part of this work has been carried out.

References

References

[1] M. Shapiro, P. Brumer, in Advances in Atomic, Molecular and Optical Physics, edited by B. Bederson and H. Walther, Vol. 42, pp. 287-345 Academic Press, San Diego, 1999.
[2] F. Ehlotzky, Phys. Rep. 345 (2001) 175.
[3] S. E. Harris, Phys. Today 50 (1997) 36.
[4] J. P. Marangos, J. Mod. Optics 45 (1998) 471.
[5] O. Kocharovskaya, Ya. I. Khanin, Sov. Phys. JETP 63 (1986) 945.
[6] K. J. Boller, A. Imamoglu, S. E. Harris, Phys. Rev. Lett. 66 (1991) 2593.
[7] G. Alzetta, A. Gozzini, L. Moi, G. Oriolis, Nuovo Cim. B 36 (1976) 5.
[8] M. Fleischhauer, A. Imamoglu, J. P. Marangos, Rev. Mod. Phys. 77 (2005) 633.
[9] A. Marian, M. C. Stowe, J. R. Lawall, D. Felinto, J. Ye, Science 306 (2004) 2063.
[10] M. C. Stowe, F. C. Cruz, A. Marian, J. Ye, Phys. Rev. Lett. 96 (2006) 153001.
[11] P. Kral, I. Thanopulos, M. Shapiro, Rev. Mod. Phys. 79 (2007) 53.
[12] E. A. Shapiro, A. Pe'er, J. Ye, M. Shapiro, Phys. Rev. Lett. 101 (2008) 023601.
[13] D. Felinto, C. A. C. Bosco, L. H. Acioli, S. S. Vianna, Opt. Commun. 215 (2003) 69.
[14] D. Felinto, L. H. Acioli, S. S. Vianna, Phys. Rev. A 70 (2004) 043403.
[15] A. A. Soares, L. E. E. de Araujo, Phys. Rev. A 80 (2009) 013832.
[16] T. Nakajima, Phys. Rev. A 64 (2001) 043406.
[17] S. E. Harris S E, Z.-F. Luo, Phys. Rev. A 52 (1995) R928.
[18] J. H. Eberly, Quantum Semiclass. Opt. 7 (1995) 373.
[19] M. D. Crisp, Phys. Rev. A 1 (1970) 1604.
[20] J. Rothenberg, D. Grischkowsky, A. Balant A, Phys. Rev. Lett. 53 (1984) 552.
[21] S. E. Harris, Phys. Rev. Lett. 70 (1993) 552.
[22] A. A. Soares, L. E. E. de Araujo, J. Phys. B: At. Mol. Opt. Phys. 43 (2010) 085003.
[23] D. D. Fröhlich, A. Kulik, B. Uebbing, A. Myssyrowicz, V. Langer, H. Stolz, W. von der Osten, Phys. Rev. Lett. 67 (1991) 2343.
[24] V. S. Egorov, V. N. Lebedev, I. B. Mekhov, P. V. Moroshkin, I. A. Chekhonin, S. N. Bagayev, Phys. Rev. A 69 (2004) 033804.

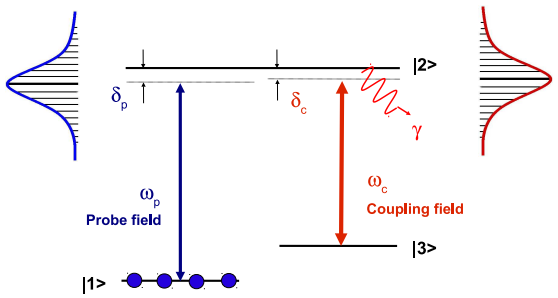

Figure 1: Level scheme for a three-level Λ-type atom interacting with the probe and coupling lasers: States $|1\rangle$ and $|2\rangle$ are coupled by a probe laser with a photon energy of ω_p, while states $|2\rangle$ and $|3\rangle$ are coupled by a coupling laser with a photon energy of ω_c. If the laser is in a form of a pulse train, the laser spectrum exhibits a frequency comb as illustrated.

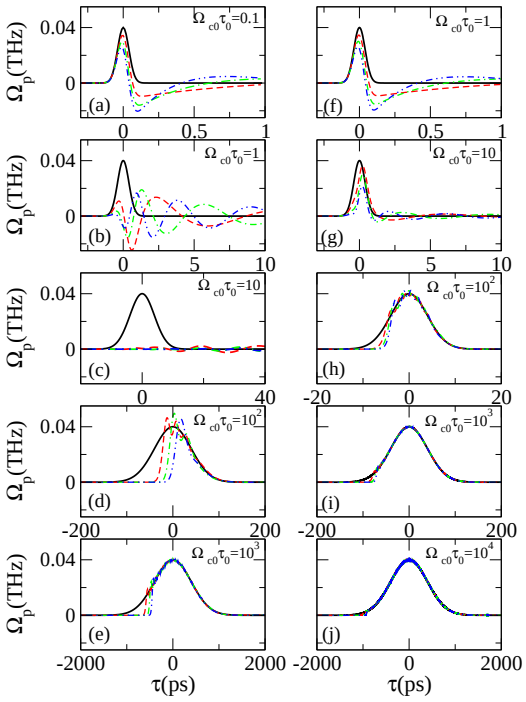

Figure 2: Temporal variation of the probe laser field $\Omega_p(\zeta,\tau)$ under the irradiation of a single pair of probe and coupling laser pulses with the durations of $\tau_0 = 100$ fs [(a) and (f)], 1 ps [(b) and (g)], 10 ps [(c) and (h)], 100 ps [(d) and (i)], and 1 ns [(e) and (j)] at different optical depths $\mu_p\zeta = 0$ (black solid line), 3 ps^{-1} (red dashed line), 6 ps^{-1} (green dot-dashed line), and 9 ps^{-1} (blue dot-dot-dashed line). The employed parameters are $\Omega_{p0} = 0.04$ THz and $\Omega_{c0} = 1$ THz for graphs (a)-(e), and $\Omega_{p0} = 0.04$ THz and $\Omega_{c0} = 10$ THz for graphs (f)-(j). For all graphs $\gamma = 70$ MHz and $\delta_p = \delta_c = 0$. (For the interpretation of the references to colour in this figure legend, the reader is referred to the web version of the paper.)

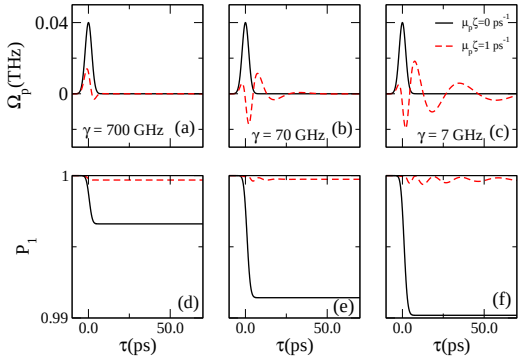

Figure 3: Temporal variation of the (a)-(c) probe laser field $\Omega_p(\zeta,\tau)$ and (d)-(f) ground state population $P_1(\zeta,\tau)$ at different optical depths $\mu_p\zeta = 0$ (solid line) and 1 ps^{-1} (dashed line), in the absence of the coupling laser field. The employed parameters are $\Omega_{p0} = 0.04$ THz, $\delta_p = 0$, $\tau_0 = 5$ ps, and $\gamma = 700$ GHz [(a) and (d)], or $\gamma = 70$ GHz [(b) and (e)], or $\gamma = 7$ GHz [(c) and (f)], which result in the pulse area of $\Omega_{p0}\tau_0 = 0.2$.

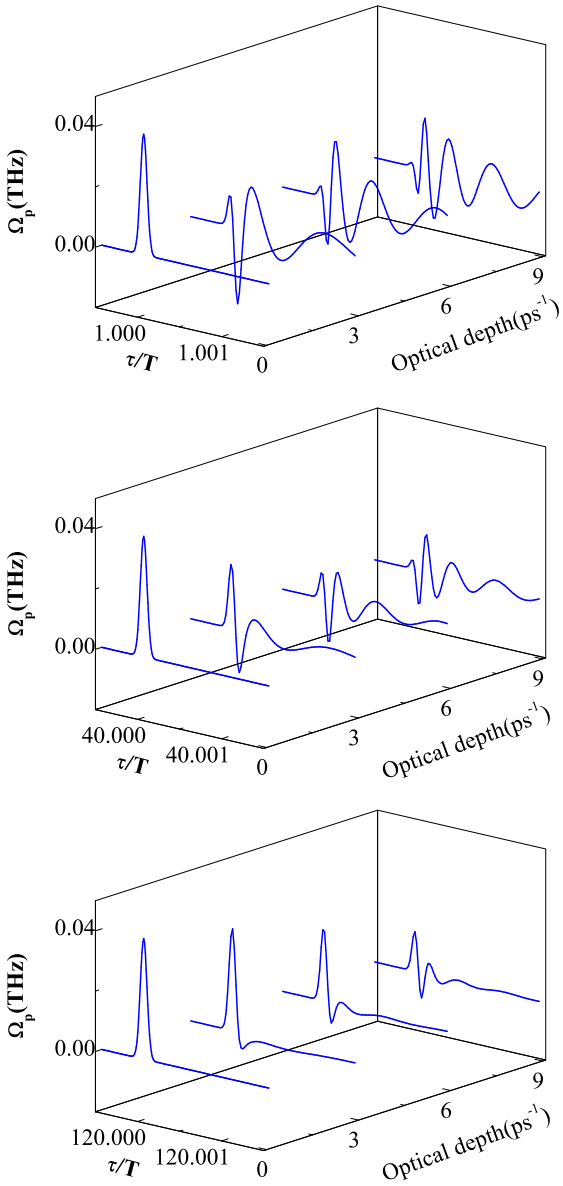

Figure 4: Spatio-temporal change of the probe laser field $\Omega_p(\zeta,\tau)$ under the presence of the coupling laser field at different optical depths $\mu_p\zeta = 0$, 3, 6, and 9 ps^{-1}. The upper, middle, and lower figures are for the first, 40^{th}, and 120^{th} pulses in the probe pulse train. The employed parameters are $\Omega_{p0} = 0.04$ THz, $\Omega_{c0} = 0.5$ THz, $\delta_p = \delta_c = 0$, $\tau_0 = 1$ ps, $T = 10$ ns, and $\gamma = 70$ MHz, which result in the pulse areas of $\Omega_{p0}\tau_0 = 0.04$ and $\Omega_{c0}\tau_0 = 0.5$.

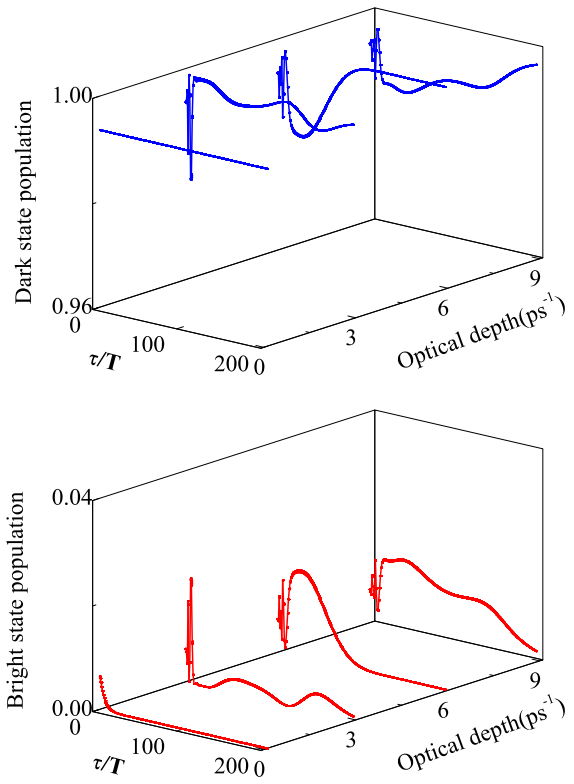

Figure 5: Spatio-temporal change of the dark and bright state populations $P_D(\zeta,\tau)$ (upper figure) and $P_B(\zeta,\tau)$ (lower figure) for different optical depths $\mu_p\zeta = 0$, 3, 6, and 9 ps^{-1}. All the parameters are the same with those for Fig. 4.

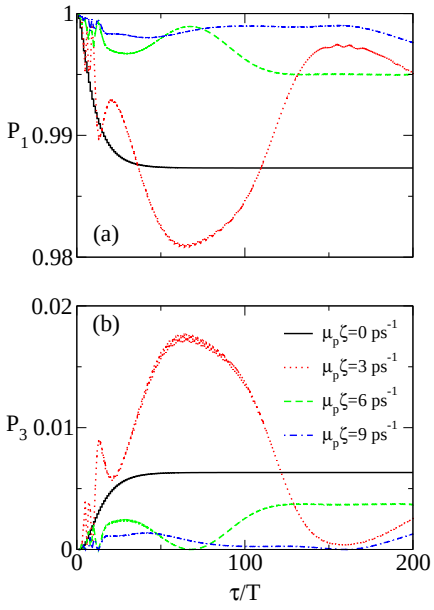

Figure 6: Ground and excited state populations $P_1(\zeta,\tau)$ and $P_3(\zeta,\tau)$ as a function of time at different optical depths $\mu_p\zeta = 0$ (black solid line), 3 ps^{-1} (red dotted line), 6 ps^{-1} (green dashed line), and 9 ps^{-1} (blue dot-dashed line). The employed parameters are the same with those for Fig. 4. (For the interpretation of the references to colour in this figure legend, the reader is referred to the web version of the paper.)

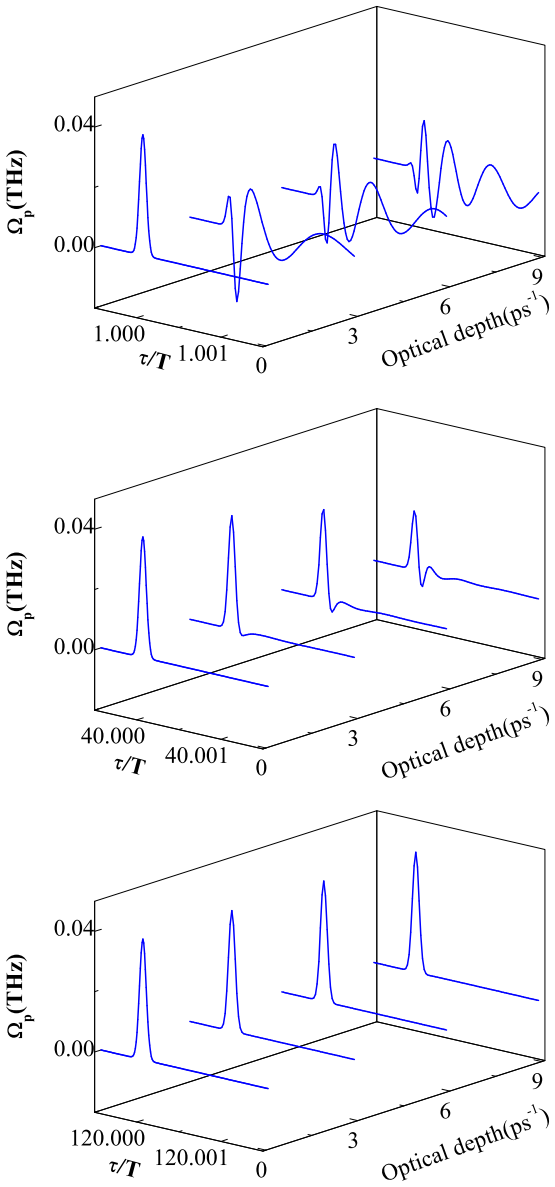

Figure 7: Similar to Fig. 4 but with $\Omega_{c0} = 1$ THz, where the rest of the parameters are the same with those for Fig. 4. Accordingly the pulse areas are $\Omega_{p0}\tau_0 = 0.04$ and $\Omega_{c0}\tau_0 = 1$.

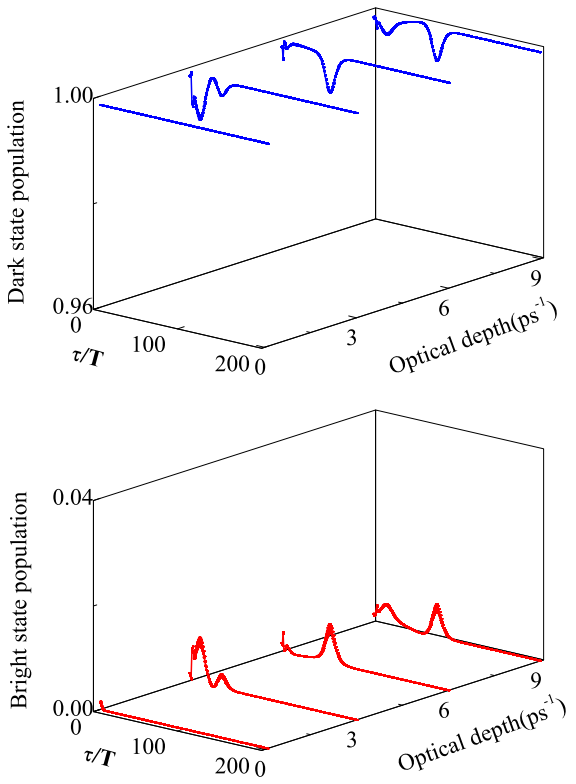

Figure 8: Spatio-temporal change of the dark and bright state populations $P_D(\zeta, \tau)$ (upper figure) and $P_B(\zeta, \tau)$ (lower figure) for different optical depths $\mu_p\zeta = 0$, 3, 6, and 9 ps^{-1}. All the parameters are the same with those for Fig. 7.

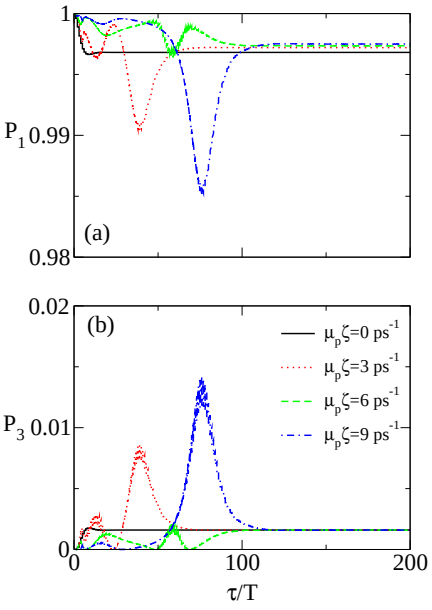

Figure 9: Ground and excited state populations $P_1(\zeta,\tau)$ and $P_3(\zeta,\tau)$ as a function of time at different optical depths $\mu_p\zeta = 0$ (black solid line), 3 ps^{-1} (red dotted line), 6 ps^{-1} (green dashed line), and 9 ps^{-1} (blue dot-dashed line). The employed parameters are the same with those for Fig. 7. (For the interpretation of the references to colour in this figure legend, the reader is referred to the web version of the paper.)

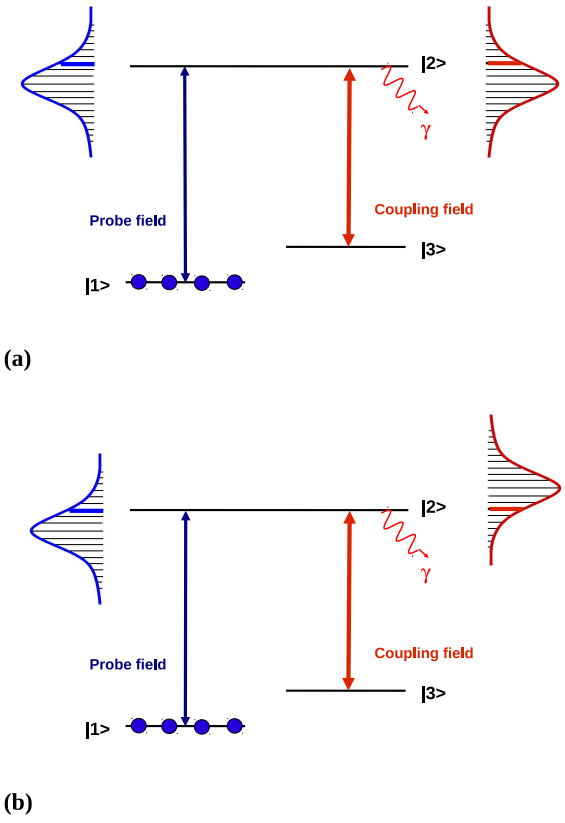

Figure 10: (Color online) Illustration of the (a) symmetric detunings $\delta_p = \delta_c$ and (b) asymmetric detunings $\delta_p = -\delta_c$. In either case one of probe as well as coupling laser comb tooth is on exact resonance with the corresponding transition.

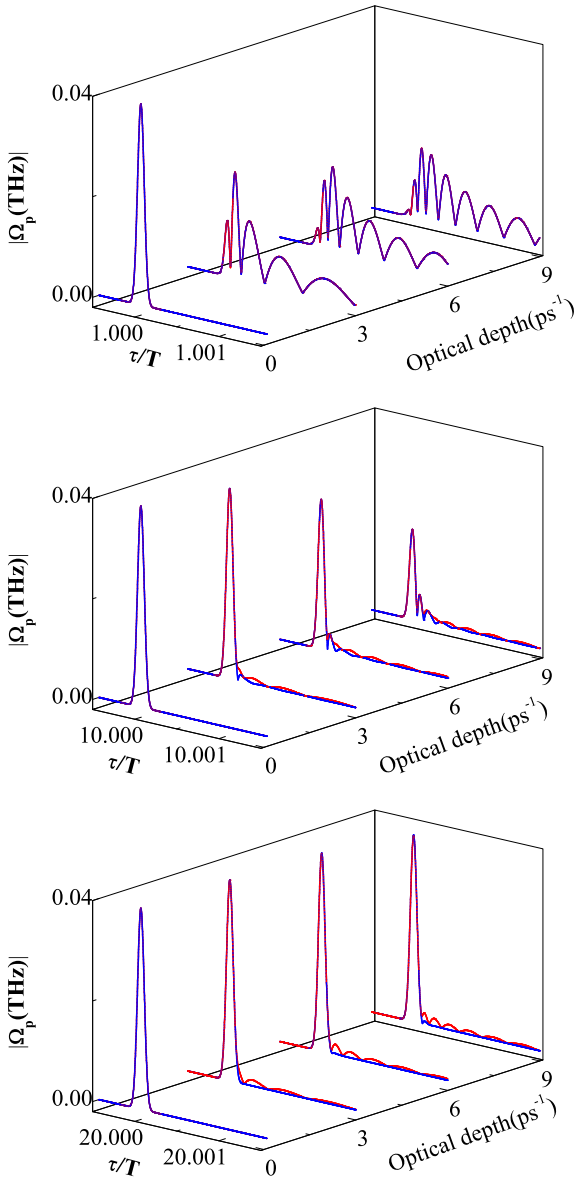

Figure 11: Spatio-temporal change of the probe laser field $|\Omega_p(\zeta,\tau)|$ at different optical depths $\mu_p\zeta$ = 0, 3, 6, and 9 ps^{-1} under the symmetric (blue lines) and asymmetric detunings (red lines). The upper, middle, and lower figures show the first, 10^{th}, and 20^{th} pulses in the probe pulse train. The choices of the symmetric and asymmetric detunings are $\delta_p = \delta_c \simeq 201.062$ GHz and $\delta_p = -\delta_c \simeq 201.062$ GHz, respectively. $\Omega_{c0} = 2$ THz, the rest of the employed parameters are the same with those for Fig. 4 and accordingly the pulse areas are $\Omega_{p0}\tau_0 = 0.04$ and $\Omega_{c0}\tau_0 = 2$. (For the interpretation of the references to colour in this figure legend, the reader is referred to the web version of the paper.)

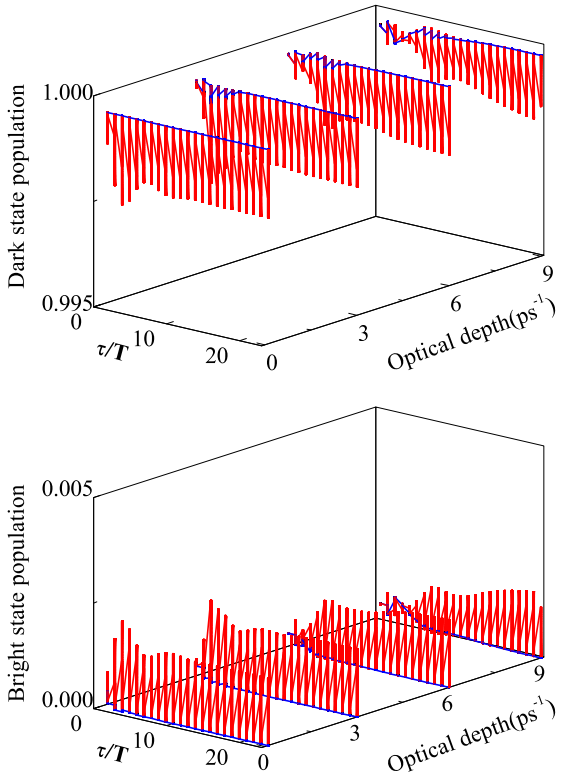

Figure 12: Spatio-temporal change of the dark and bright state populations $P_D(\zeta,\tau)$ (upper figure) and $P_B(\zeta,\tau)$ (lower figure), for different optical depths $\mu_p\zeta$ = 0, 3, 6, and 9 ps^{-1}, under the symmetric (blue lines) and asymmetric detunings (red lines, see-saw pattern). All the parameters are the same with those for Fig. 11. (For the interpretation of the references to colour in this figure legend, the reader is referred to the web version of the paper.)

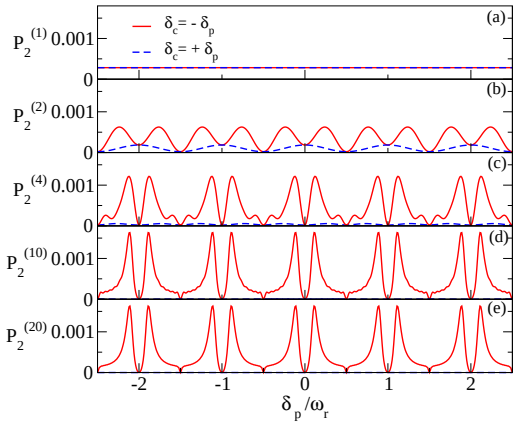

Figure 13: Population of the upper excited state P_2 as a function of the probe laser detuning, at optical depth $\mu_p\zeta = 0$, under symmetric (blue dashed lines) and asymmetric detunings (red solid lines) for the first (a), 2^{nd} (b), 4^{th} (c), 10^{th} (d), and 20^{th} (e) probe pulse in the train. All the parameters are the same with those for Fig. 11. (For the interpretation of the references to colour in this figure legend, the reader is referred to the web version of the paper.)